CDF 9/7 Wavelets as Sparsifying Operator in Compressive Holography

Yan, Hao; Blinder, David; Bettens, Stijn; Ottevaere, Heidi; Munteanu, Adrian; Schelkens, Peter

Published in:
IEEE International Conference on Image Processing 2015

DOI:
10.1109/ICIP.2015.7351154

Publication date:
2015

Document Version:
Accepted author manuscript

CDF 9/7 Wavelets as Sparsifying Operator in Compressive Holography

Hao Yan[1,4], David Blinder[1,3], Stijn Bettens[1,3], Heidi Ottevaere[2], Adrian Munteanu[1,3] and Peter Schelkens[1,3*]
[1] Vrije Universiteit Brussel, Department of Electronics and Informatics (ETRO), Pleinlaan 9, 2-1050 Brussels, Belgium
[2] Vrije Universiteit Brussel, Brussels Photonics Team (B-PHOT), Pleinlaan 2, B-1050 Brussels, Belgium
[3] iMinds, Department of Multimedia Technologies (MMT), Gaston Crommenlaan 8 (box 102), B-9050 Ghent, Belgium
[4] Shanghai Jiao Tong University, Department of Instrument Science and Engineering, School of EIEE, Shanghai 200240, China
Corresponding email: pschelke@etro.vub.ac.be*

ABSTRACT

Compressive sensing is a mathematical framework, which seeks to capture the information of an object using as few measurements as possible. Recently, it has been applied to holography, where the most frequently used reconstruction method is l_1-norm minimization with the Haar wavelet as the sparsifying operator. In this work, we promote the CDF 9/7 wavelet as the sparsifying operator. We demonstrate that the CDF 9/7 wavelet performs better than the Haar wavelet.

Index Terms— *compressive sensing, compressive Fresnel holography, Haar wavelet, CDF 9/7 wavelet.*

1. Introduction

Compressive Sensing (CS) is a mathematical framework for sampling and reconstructing signals [1]. It allows for the accurate reconstruction of a signal from a substantially smaller number of samples than required by the Shannon-Nyquist sampling theorem in the case of uniform sampling by exploiting the signal's inherent sparsity.

Recently, CS has been successfully introduced in holographic imaging [2, 3]. The sensing operator deployed in holographic CS is the free-space wave propagation, which is mathematically expressed by the Fresnel transform. As the Fresnel transform is closely related to the Fourier transform – a common sensing operator in CS – it fits well in the CS framework [4].

The application of CS in holography, which is also referred to as compressive holography (CH), has led to remarkable achievements including the recovery of partially occluded objects [5, 6], 3D tomography of non-diffuse [2] and diffuse objects [7], enhancement of the axial resolution of in-line holography [8, 9], multidimensional optical information acquisition [10], reducing scanning effort in incoherent multiple view projection holography [11] and digital holography with a single-pixel detector [12].

According to CS theory, the effectiveness and quality of CS reconstruction greatly depends on the sparsity of the underlying signal. The sparser the signal can be represented, the better the achievable reconstruction quality will be. Hence, its sparsity is determined by the type of sparsifying operator applied and the corresponding sparse basis. Until now, the Haar wavelet transform is the most used sparsifying operator in CS due to its simple implementation. However, seen the short support width of this wavelet basis, it is to be expected that its sparsifying performance is not optimal for more complex signals than for example a simple piece-wise constant (PWC) object/image, i.e. objects/images that depict a 'binary' structure. Hence, to improve the effectiveness and quality of CS reconstruction, investigation of other sparsifying operators is necessary.

In this paper, we promote the Cohen-Daubechies-Feauveau (CDF) 9/7 wavelet [13-15] as a sparsifying operator. Compared to Haar, it concentrates more energy in the lower frequency subbands. This characteristic results in the improved preservation of object information in CH.

In the next sections, we will first shortly introduce compressive sensing theory. Section 3 will cover compressive Fresnel holography and describe the compressive sensing framework that has been implemented. Subsequently, Section 4 will address the experiments and finally, Section 5 will draw the conclusions.

2. Compressive Sensing Theory

CS theory relies on two conditions: the inherent signal's sparsity and the incoherence between the sparsifying and sensing operators. To simplify the explanation of CS theory, let us consider an object f being projected to g by a sensing operator ϕ and being sparsely represented in an arbitrary basis ψ. The sensing mechanism can be expressed by Eq. (1).

$$g = \phi f = \phi\psi\alpha \tag{1}$$

where α is the S-sparse representation of f with sparse operator ψ and S is the number of non-zero coefficients of α. Due to the homogeneous, compact and regular structure of the considered objects, most images are sparse in their original or transformed domain (e.g., wavelet domain). If the sensing operator is (approximately) incoherent with the sparse operator, the CS framework can be applied. A highly accurate CS reconstruction can be achieved by l_1-norm minimization by solving the following convex optimization problem [1]:

$$\hat{\alpha} = \min_{\alpha} \|\alpha\|_{l1} \quad \text{subject to} \quad g = \phi\psi\alpha, \tag{2}$$

given that the sampling criterion in Eq.(3) is satisfied:

$$M \geq KS\mu \log(N) \quad (3)$$

where M is the number of pixels in the subsampled version of g in the CS sampling framework and N is the number of pixels of the image f. K is a constant and S is the number of the non-zero coefficients of α. μ represents the coherence between the sensing and sparsifying operators.

3. Compressive Fresnel Holography (CFH)

The sensing operator ϕ in CH is free-space wave propagation. Hologram recording in the Fresnel diffraction region is called Fresnel holography [16]. In this case, □ is a Fresnel transform, which relates the object f to the complex wavefield g in the measurement plane perpendicular to the propagation direction at distance z. Consequently, Eq. (1) canbe further expanded by the Fresnel transform as:

$$g = \phi f = A\exp\left\{\frac{j\pi}{\lambda z}x^2\right\}\int_{-\infty}^{+\infty} f(\xi)\exp\left\{\frac{j\pi}{\lambda z}\xi^2\right\}\exp\left\{\frac{-j2\pi}{\lambda z}x\xi\right\}d\xi \quad (4)$$

The discrete form of the Fresnel transform and the inverse Fresnel transform can be found in [3] and [17]. We refer to the conventional reconstruction method of Eq. (4) as the back propagation (BP) method. Both in-line phase-shifting and off-axis holography configurations can be used to acquire the complex wavefield g [18]. In this work, an off-axis holography configuration is adopted for the acquisition of the complex wavefield g.

In CFH, only g_M, a subsampled set of g, is used. CS reconstruction will allow for finding the best estimator $\hat{f} = \psi\hat{\alpha}$ of f by solving the convex optimization problem in Eq. (2). In this work, Eq. (2) is solved by the Projection Over Convex Sets (POCS) algorithm, which iterates between soft-thresholding and imposing data consistency in the measurement domain [19]. Its flow chart is given in Fig. 1 where $\hat{g}$ is defined as the undersampled Fresnel transform of the estimator $\hat{f}$. $\hat{\alpha}_0 = \psi^{-1}\phi^{-1}g_M$ is used as initial setting for the iteration.

According to Eq. (3), the smallest number of measurements M needed for CS reconstruction is determined by the image sparsity S in the sparse domain. Suitable sparse bases ψ are those providing smaller values of S. Eq. (3) also indicates that, for some number of measurements M, sparser bases provide better image quality after CS reconstruction. In this work, we investigate the performance differences between CDF 9/7 and the frequently used Haar wavelets as sparsifying basis in CFH and analyze the reasons behind the differences.

4. Experimental Validation

In this part, we compare the Haar and CDF 9/7 wavelets for CS reconstruction. The Haar wavelets are the simplest wavelets and are considered as a suitable basis for sparse representation of relatively simple objects such as piece-wise constant (PWC) specimens. Currently, the Haar basis is the most frequently used wavelet basis in CFH.

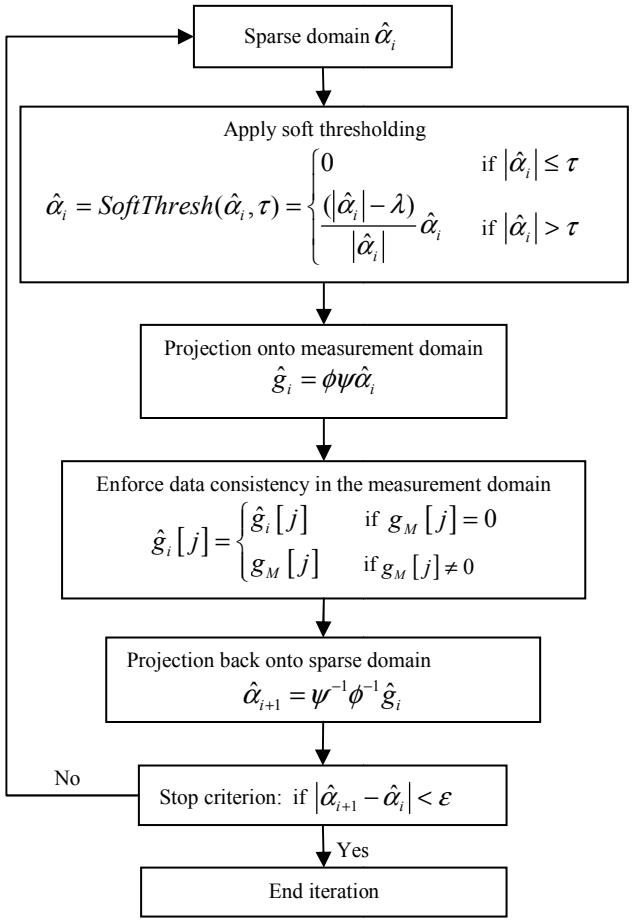

Fig.1 Flow chart of the implementation of Eq. (2) with POCS.

4.1 Evaluation of Haar and CDF 9/7 Transforms as Sparsifying Operators

A first illustrative experiment is performed with an image of a PWC specimen, the USAF (US Air Force) 1951 target (Fig. 2), which is an amplitude pattern with bright parts of amplitude one and dark parts of amplitude zero.

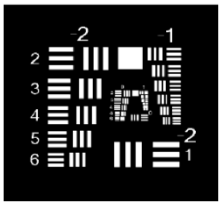

Fig. 2 The USAF 1951 target (1024x1024 pixels).

We apply the Haar and CDF 9/7 wavelet transforms on this image. Its sparsity in the wavelet domain is evaluated with the l_0-norm $\|\alpha\|_{l0}$ and the l_1-norm $\|\alpha\|_{l_1}$ of both transforms; the smaller $\|\alpha\|_{l0}$ and $\|\alpha\|_{l_1}$, the larger the sparsity. As a result, we obtain $\|\alpha_{haar}\|_{l0} = 4688$, $\|\alpha_{CDF9/7}\|_{l0} = 28032$ (at Matlab precision), $\|\alpha_{haar}\|_{l1} = 2645$ and $\|\alpha_{CDF9/7}\|_{l1} = 3255$

for a total of N=1024*1024 pixels. Therefore, the Haar wavelet is a better sparsifying operator than the CDF 9/7 wavelet for this ideal PWC specimen.

In the next holographic recording experiment, we use the USAF 1951 target as specimen, which is a PWC object similar to the one used in the simulation. In this particular experiment, we use an off-axis geometry for hologram recording [20]. In-line phase-shifting geometry is possible as well. Both are only tools to obtain the complex wavefront g in Eq. (4). The amplitude of g is shown in Fig. 3 (a). The reconstructed complex wavefield f is obtained with Eq. (4). The center part of the reconstructed amplitude image $|f|$ is presented in Fig. 3 (c). In this paper, for illustrative purposes, only the center parts of the reconstructed images are presented. However, for measurements and calculations, the full image data were used.

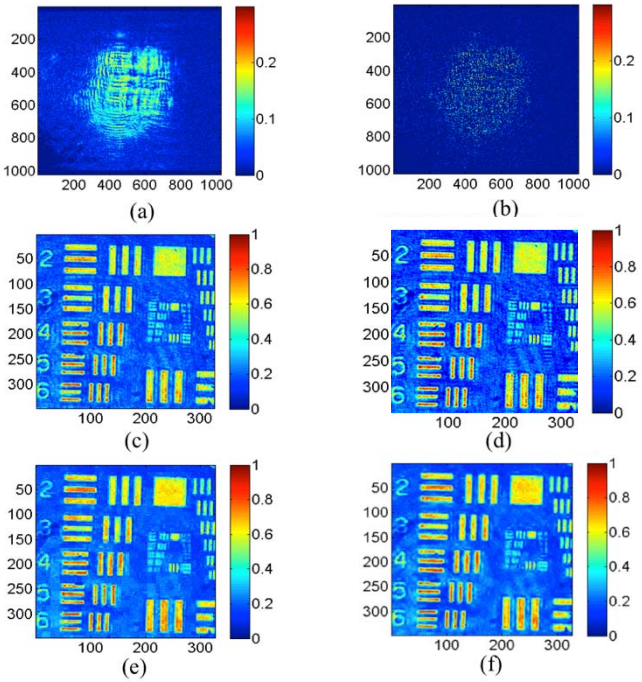

Fig. 3 (a) Amplitude of wavefront g; (b) amplitude of g_M (15 % subsampling rate); (c) reconstruction by BP from g; (d) reconstruction by interpolated BP from g_M; (e) CS with Haar wavelet; (f) CS with CDF 9/7 wavelet.

First, the Haar and CDF 9/7 wavelet transforms of f are calculated to compare their performances as sparse operators. The two transforms are shown in respectively, Fig. 4 (a) and (b). It can be easily noticed that the signal is sparser in the CDF 9/7 domain (b) than in the Haar domain (a). To quantify the sparsity, $\|\alpha\|_{l_1}$ is calculated and it turns out that $\|\alpha_{haar}\|_{l1} = 2.0768\times10^4$ and $\|\alpha_{CDF9/7}\|_{l1} = 1.7319\times10^4$ with $\|\alpha_{haar}\|_{l1} / \|\alpha_{CDF9/7}\|_{l1} = 1.43$. Therefore, the CDF 9/7 wavelet performs better than the Haar wavelet as a sparsifying operator for this PWC object in a practical experimental setting, which is opposite to the simulation results in the first experiment. The non-perfect PWC behavior of the reconstructed image results in a reduced performance of the Haar wavelet as sparsifying basis.

This demonstrates that the small changes in image properties due to the measurement set-up and potential associated imperfections give rise to a difference between the

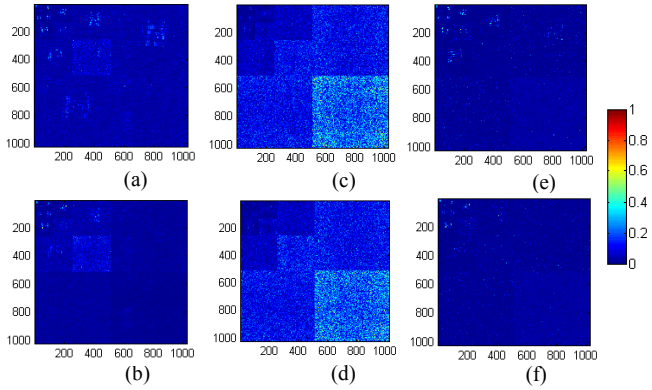

simulation and the experimental results. Hence, this is a first indication to give preference to the CDF 9/7 wavelet transform as the sparsifying operator rather than the Haar wavelet.

We further examine the Haar and CDF 9/7 wavelets as sparsifying operators for the holographic recording of a non-PWC constant object: a spherical reflective surface. Its BP reconstruction with full sampling is shown in Fig. 6 (a) on which the Haar and CDF 9/7 wavelet transforms are deployed. The ratio $\|\alpha_{haar}\|_{l1} / \|\alpha_{CDF9/7}\|_{l1}$ is 2.12 in this case. Therefore, the CDF 9/7 wavelets perform even better than the Haar wavelets as a sparsifying operator for this non-PWC object.

Fig. 4 (a) Haar and (b) CDF 9/7 wavelet transform of the image reconstructed f by BP from g; (c) Haar and (d) CDF 9/7 wavelet transform of the image reconstructed by BP from g_M (15% subsampling rate); (e) Haar and (f) CDF 9/7 transform of the image reconstructed by CS from g_M.

4.2 CS reconstruction of both the PWC and non-PWC objects

Firstly, the complex wavefront g in Fig. 3 (a) is randomly and uniformly subsampled (15%) resulting in g_M Fig. 3 (b). We subsequently applied the BP reconstruction of Eq. (4) and the CS reconstruction introduced in Section 3 on the subsampled complex wavefront. The results of BP, CS with Haar wavelets and CS with CDF 9/7 wavelets on g_M are presented in respectively Fig. 3 (d), (e) and (f). It can be observed that both CS reconstructions result in a smoother approximation than the BP method, which is more crisp in nature. To quantify the reconstruction quality, we calculate the PSNRs of the amplitude images. For each reconstruction method, the reconstructed amplitude image with 99% sam-

pling rate is used as the reference. The PSNR is defined as $10\times\log_{10}(MAX_I^2/MSE)$, where MSE is the mean squared error of the pixel-wise differences between the reconstructed and the reference image of the corresponding method. MAX_I is the maximum value of the reference image. With different subsampling rates, the PSNRs of the BP, interpolation BP (which deploys BP on the cubicly interpolated wavefront), CS Haar and CS CDF 9/7 reconstructed amplitude images are calculated and shown in Fig. 6. Each PSNR is obtained by averaging the PSNRs of ten repetitive experiments with the same sampling rate but different random sampling masks. The variances of repetitive measurements at the different sampling rates are very low (~10^{-4} dB^2). We observe that the two CS reconstructions and interpolation BP are much better than the direct BP method, and that the CDF 9/7 wavelets perform better than Haar wavelets and BPP interpolation for all the sampling rates.

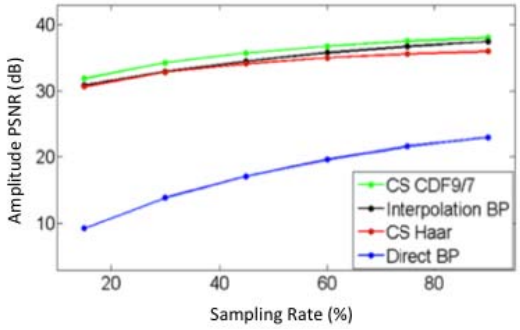

Fig. 5 PSNR of amplitude images at different sampling rates.

At the same time, the impact of subsampling is also investigated. The Haar and CDF 9/7 transforms of Fig. 3 (d) are presented in Fig. 4 (c) and (d). The Haar transform of Fig.3 (e) and the CDF 9/7 transform of Fig.3 (f) are presented in Fig.5 (e) and (f) respectively. By comparing Fig. 4 (a) to (d), it can be observed that the impact of the subsampling of the complex wavefront results in large noise interference in the sparse domain. However, CS reconstruction in Fig.4 (e) and (f), suppresses the noise such that useful information emerges. As CDF 9/7 concentrates more useful information in the lower frequency subbands as in Fig. 5 (b), it performs better under noisy conditions.

Additionally, we perform the CS reconstruction of the non-PWC constant object: a spherical reflective surface. With 15% subsampling, the images of the BP with interpolation, CS Haar and CS CDF 9/7 reconstructions are shown in Fig. 6 (b) to (d). The PSNRs of the amplitude images with different subsampling rates and different reconstruction algorithms are evaluated and shown in Fig.6 (e). Each PSNR is obtained the same way as in Fig. 5 by averaging ten repetitive measurements. The variances of repetitive measurements at the different sampling rates are very low as well (10^{-4} dB^2). It can be seen that CS reconstructions are much better than the BP reconstruction, which is more crisp. It should be noted here as well that for very high-frequent content (e.g. when using greater recording angles in the off-axis recording set-up) conventional interpolation might become problematic. The CDF 9/7 performs better than the Haar and is less sensitive to subsampling. The curve indicates that the Haar wavelet performance immediately drops due to the fact even little subsampling has immediately an impact on the achievable reconstruction quality. CDF 9/7's behavior is more stable.

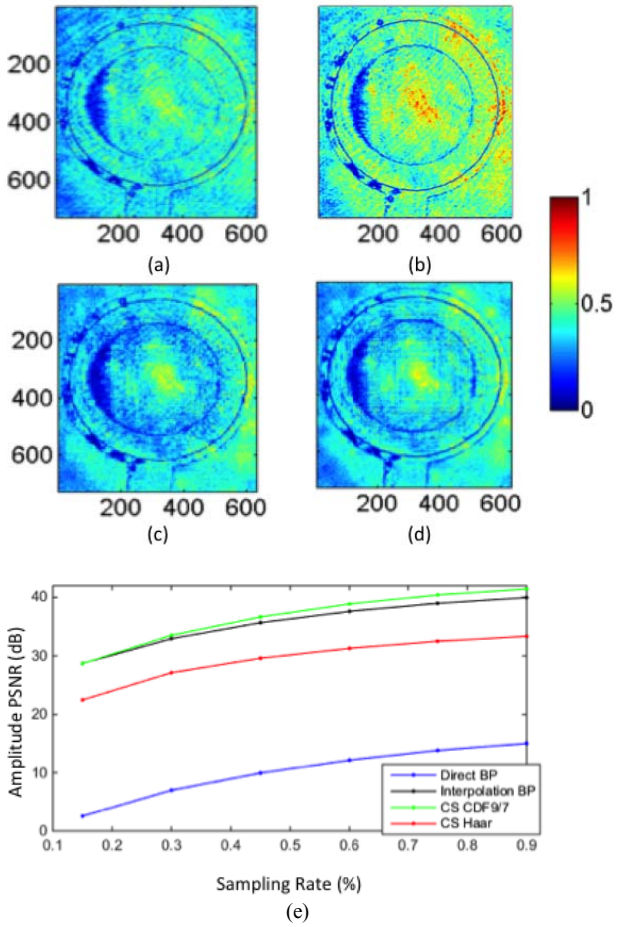

Fig. 6 (a) Reconstruction by BP with full wavefront sampling; (b) reconstruction by BP with 15% wavefront subsampling; (c) reconstruction by CS with Haar with 15% subsampling; (d) reconstruction by CS with CDF 9/7 with 15% subsampling; (e) PSNR of amplitude images at different sampling rates.

5. Conclusions

In this work, we have introduced a CFH reconstruction framework with l_1-norm minimization supporting both Haar and CDF 9/7 wavelets. We have proven for 2 test objects that the CDF 9/7 wavelet performs better than the Haar wavelet as sparsifying operator. It depicts a much more stable behavior and retains the image structures more accurately.

6. Acknowledgments

The research leading to these results has received funding from the European Research Council under the European Union's Seventh Framework Programme (FP7/2007-2013)/ERC Grant Agreement n. 617779 (INTERFERE) and

the National Natural Science Foundation of China (Grant No. 61405111).

7. References

[1] E. J. Candès and M. B. Wakin, "An introduction to compressive sampling," *IEEE Signal Processing Magazine,* vol. 25, pp. 21-30, Mar 2008.

[2] D. J. Brady, K. Choi, D. L. Marks, R. Horisaki, and S. Lim, "Compressive Holography," *Optics Express,* vol. 17, pp. 13040-13049, Jul 2009.

[3] Y. Rivenson, A. Stern, and B. Javidi, "Compressive Fresnel Holography," *Journal of Display Technology,* vol. 6, pp. 506-509, Oct 2010.

[4] Y. Rivenson and A. Stern, "Conditions for practicing compressive Fresnel holography," *Optics Letters,* vol. 36, pp. 3365-3367, Sep 1, 2011.

[5] Y. Rivenson, A. Rot, S. Balber, A. Stern, and J. Rosen, "Recovery of partially occluded objects by applying compressive Fresnel holography," *Optics Letters,* vol. 37, pp. 1757-1759, May 15, 2012.

[6] Y. Rivenson, A. Stern, and B. Javidi, "Overview of compressive sensing techniques applied in holography," *Applied Optics,* vol. 52, pp. A423-A432, Jan 1, 2013.

[7] K. Choi, R. Horisaki, J. Hahn, S. Lim, D. L. Marks, T. J. Schulz*, et al.*, "Compressive holography of diffuse objects," *Applied Optics,* vol. 49, pp. H1-H10, Dec 2010.

[8] X. Wu, Y. Yu, W. Zhou, and A. Asundi, "4f amplified in-line compressive holography," *Optics Express,* vol. 22, pp. 19860-19872, Aug 25 2014.

[9] Y. Rivenson, A. Stern, and B. Javidi, "Improved depth resolution by single-exposure in-line compressive holography," *Applied Optics,* vol. 52, pp. A223-A231, Jan 1, 2013.

[10] R. Horisaki, J. Tanida, A. Stern, and B. Javidi, "Multidimensional imaging using compressive Fresnel holography," *Optics Letters,* vol. 37, pp. 2013-2015, Jun 1, 2012.

[11] Y. Rivenson, A. Stern, and J. Rosen, "Compressive multiple view projection incoherent holography," *Optics Express,* vol. 19, pp. 6109-6118, Mar 28, 2011.

[12] P. Clemente, V. Duran, E. Tajahuerce, P. Andres, V. Climent, and J. Lancis, "Compressive holography with a single-pixel detector," *Optics Letters,* vol. 38, pp. 2524-2527, Jul 2013.

[13] D. Blinder, T. Bruylants, E. Stijns, H. Ottevaere, and P. Schelkens, "Wavelet Coding of Off-axis Holographic Images," *Applications of Digital Image Processing XXXVI,* vol. 8856, 2013 .

[14] T. Bruylants, D. Blinder, H. Ottevaere, A. Munteanu, and P. Schelkens, "Microscopic Off-axis Holographic Image Compression with JPEG 2000," *Optics, Photonics, and Digital Technologies for Multimedia Applications III,* vol. 9138, 2014 .

[15] D. Blinder, T. Bruylants, H. Ottevaere, A. Munteanu, and P. Schelkens, "JPEG 2000-based compression of fringe patterns for digital holographic microscopy," *Optical Engineering,* vol. 53, Dec 2014.

[16] J. W. Goodman, *Introduction to Fourier Optics,* 1996.

[17] M. M. Marim, M. Atlan, E. Angelini, and J.-C. Olivo-Marin, "Compressed sensing with off-axis frequency-shifting holography," *Optics Letters,* vol. 35, pp. 871-873, Mar 15, 2010.

[18] M. Marim, E. Angelini, J.-C. Olivo-Marin, and M. Atlan, "Off-axis compressed holographic microscopy in low-light conditions," *Optics Letters,* vol. 36, pp. 79-81, Jan 2011.

[19] M. Lustig, D. Donoho, and J. M. Pauly, "Sparse MRI: The application of compressed sensing for rapid MR imaging," *Magnetic Resonance in Medicine,* vol. 58, pp. 1182-1195, Dec 2007.

[20] H. Yan and A. Asundi, "Studies on aperture synthesis in digital Fresnel holography," *Optics and Lasers in Engineering,* vol. 50, pp. 556-62, April 2012.